Published in final edited form as:
Bone. 2013 February ; 52(2): 712–717. doi:10.1016/j.bone.2012.07.029.

Raman spectroscopy demonstrates Amifostine induced preservation of bone mineralization patterns in the irradiated murine mandible

Catherine N. Tchanque-Fossuo[#a], **Bo Gong**[#b], **Behdod Poushanchi**[a], **Alexis Donneys**[a], **Deniz Sarhaddi**[a], **K. Kelly Gallagher**[c], **Sagar S. Deshpande**[a], **Steven A. Goldstein**[d], **Michael D. Morris**[b], and **Steven R. Buchman**[a,*]

[a]University of Michigan Hospital and Health Systems, Pediatric Plastic Surgery Section, 1540 E. Hospital Drive, MI 48109, USA

[b]University of Michigan Hospital and Health Systems, Department of Chemistry, 930 N. University, Ann Arbor, MI 48109, USA

[c]University of Michigan Hospital and Health Systems, Department of Otolaryngology–Head and Neck Surgery, University of Michigan Medical School, 1500 E. Medical Center Drive, Ann Arbor, MI 48109, USA

[d]University of Michigan, Department of Orthopaedic Surgery, A. Alfred Taubman Biomedical Science Research Building, 109 Zina Pitcher Pl, Ann Arbor, MI, 48109, USA

[#] These authors contributed equally to this work.

Abstract

Purpose—Adjuvant radiotherapy in the management of head and neck cancer remains severely debilitating. Fortunately, newly developed agents aimed at decreasing radiation-induced damage have shown great promise. Amifostine (AMF) is a compound, which confers radio-protection to the exposed normal tissues, such as bone. Our intent is to utilize Raman spectroscopy to demonstrate how AMF preserves the mineral composition of the murine mandible following human equivalent radiation.

Methods—Sprague Dawley rats were randomized into 3 experimental groups: control (n=5), XRT (n=5), and AMF–XRT (n=5). Both XRT and AMF groups underwent bioequivalent radiation of 70 Gy in 5 fractions to the left hemimandible. AMF–XRT received Amifostine prior to radiation. Fifty-six days post-radiation, the hemimandibles were harvested, and Raman spectra were taken in the region of interest spanning 2 mm behind the last molar. Bone mineral and matrix-specific Raman bands were analyzed using one-way ANOVA, with statistical significance at $p<0.05$.

Results—The full-width at half-maximum of the primary phosphate band (FWHM) and the ratio of carbonate/phosphate intensities demonstrated significant differences between AMF–XRT versus XRT ($p<0.01$) and XRT versus control ($p<0.01$). There was no difference between AMF–XRT and control ($p>0.05$) in both Raman metrics. Computer-aided spectral subtraction further

[*]Corresponding author at: Craniofacial Anomalies Program, University of Michigan Hospital and Health Systems, Pediatric Plastic Surgery Section, 4-730, C.S. Mott Children's Hospital, 1540 E. Hospital Drive, Ann Arbor, MI 48109-4215, USA. Fax: +1 734 936-7815. sbuchman@umich.edu.

Disclosures Michael D. Morris receives consulting income from Kaiser Optical Systems, Inc.; the rest of the authors have no conflicts of interest.

confirmed these results where AMF–XRT was spectrally similar to the control. Interestingly, the collagen cross-link ratio did not differ between XRT and AMF–XRT ($p<0.01$) but was significantly different from the control ($p<0.01$).

Conclusion—Our novel findings demonstrate that AMF prophylaxis maintains and protects bone mineral quality in the setting of radiation. Raman spectroscopy is an emerging and exceptionally attractive clinical translational technology to investigate and monitor both the destructive effects of radiation and the therapeutic remediation of AMF on the structural, physical and chemical qualities of bone.

Keywords

Amifostine; Raman spectroscopy; Mandible; Bone mineral composition

Introduction

The clinical management of head and neck malignancies conventionally involves surgical extirpation of the tumors, adjuvant radiation and facial reconstruction. Radiotherapy has contributed with impressive strides to the cure rates observed in patients afflicted by such illness. Nonetheless, radiation is associated with acute and late toxicities to the adjacent non-cancerous tissues and organs. Those unfortunate complications involve oral mucositis, xerostomia, pathologic fractures and osteoradionecrosis, which are severely debilitating to the patients. We have undertaken to investigate a chemical protectant that would be able to remediate both the early and late ravaging sequelae induced by radiation. Amifostine or AMF (WR-2721, Ethyol, MedImmune, Gaithersburg, MD) is one such chemical, of thousands screened by the Walter Reed Army Institute of Research that demonstrated a range of radioprotection properties [1–3]. Among all those compounds, AMF was found to selectively protect the normal tissues from the unwarranted effects of both radiation and antineoplastic agents [3]. AMF's superior protection to the normal cells was associated with acceptable toxicity. The mechanism of action of the pro-drug AMF or WR-2765 resides in its conversion by the cell membrane-bound alkaline phosphatase into the cyto-protective thiol metabolite WR-1065 [1–5]. The active free sulfyhydryl WR-1065 reverses radiation-induced damage to the tissue cellular constituents. In the setting of ionizing radiation, free radicals are generated on cellular DNA, which subsequently breaks or may create reactive species that further adversely interact with DNA [1–5]. WR-1065 scavenges those free radicals, and donates hydrogen ions that will contribute to DNA repair and stabilization [1–5]. The selectivity of AMF to normal tissue quickly led to clinical trials for chemotherapy and radiotherapy and ultimately FDA approved labeling for protection against cisplatin-induced nephrotoxicity in ovarian cancer or non-small-cell lung cancer and radiation-induced xerostomia in head and neck cancer [6,7]. AMF was of great interest to our laboratory, as we could strategically utilize its pharmacokinetics to effectively mitigate the devastating effects of radiation on bone healing and repair and ultimately optimize bone regeneration via distraction osteogenesis [8].

Utilizing micro-computed tomography, our laboratory evaluated AMF prophylactic therapy on bone following a fractionated human equivalent dose of radiation (HEDR) [8–11]. Standard radiomorphometrics demonstrated a significant increase in bone mineral density, tissue mineral density and bone volume fraction in the radiated specimens compared to the AMF-pretreated ones. The results seemed counter-intuitive since radiation typically weakens the bone by decreasing its mineral density. Looking beyond the standard radiomorphometrics, specifically at bone mineral density distribution histograms we were able to delineate and quantify some of the pernicious effects of radiation on bone mineral profile. We learned that radiation blunted remodeling, inhibited new bone formation and

caused a significant shift towards hypermineralization. On the other hand, AMF demonstrated a significant increase in low mineralized bone compared to the irradiated hemimandibles. However, the AMF level was only slightly over half of the normal non-irradiated bone level in the lower spectrum. Therefore, AMF enabled the recruitment of bone cells to remediate to some extent the radiation-induced deleterious effect on new bone formation.

Because bone is a complex tissue, these important results prompted us to evaluate and further quantify the effects of AMF on bone utilizing Raman spectroscopy. Raman spectroscopy is a methodology that allows us to examine changes in composition, crystallinity and other properties of the organic and inorganic components of bone [12,13]. It has become increasingly popular among bone research over the past decade [12]. Developments in fiber-optic probes have shown the potential for non-invasive Raman spectroscopy of bone tissue [12–18]. Shifts in peaks corresponding to particular components of the bone give us insight into the detailed pathophysiology of the events that occur when a bone undergoes radiation [12,19–21]. As a complex composite material, the bone contains a mineral component, an organic matrix and water. The mineral is a poorly crystalline hydroxyapatite ($Ca_{10}(PO_4)_6(OH)_2$) with partial substitution of phosphate (B-type) and hydroxyl (A-type) by carbonate, and with small amounts of other cations and anions [22–24]. The matrix is mostly type I collagen with contributions (~10%) from other proteins, and proteoglycans, including bone sialoprotein, osteocalcin and osteopontin [25,26]. These non-collagenous components are involved in controlling mineralization and some are also responsible for binding the mineral to the matrix [27,28]. Water accounts for ~20% of the weight of fresh bone tissue. Both mineral and organic parts give specific Raman features which closely relate to bone quality and disease [12,19,20]. In particular, Raman spectroscopy has been used to elucidate composition effects on bone biomechanics [29–33], by utilizing co-localization of Raman spectroscopic and nano-indentation measurements [34]. We hypothesize that Raman spectroscopy will illustrate and validate AMF's preservative capabilities both in the collagen matrix (organic) and mineral (inorganic) components of bone quality and strength following human equivalent radiation. Non-invasive Raman spectroscopy has already been demonstrated in model systems as well as in animals and the technology is currently under intensive development [13–18]. This work suggests the potential translational utility of spectroscopy to monitor the course of adjuvant therapy in human subjects.

Materials and methods

Fifteen adult male Sprague Dawley rats weighing approximately 400 g were obtained through the University of Michigan's Unit for Laboratory Animal Medicine (ULAM). Prior to handling, the animals had a 7-day acclimation interval period. These animals were randomly assigned to three experimental groups. Group 1 (n=5) was a standard control and did not receive any radiation and/or treatment. Group 2, XRT (n=5) underwent radiation; Group 3, AMF–XRT (n=5) received a prophylactic treatment of AMF (100 mg/kg; Ethyol, MedImmune, Gaithersburg, MD) subcutaneously 45 min prior to radiation [35,36]. The animals were kept in a pathogen-free facility on a 12-hour light/dark schedule. Prior to handling and radiation, the rats had a 7-day acclimation period. The University of Michigan's Committee for the Utilization and Care of Animals (UCUCA) approved all studies.

Radiation

An oxygen–isoflurane mixture was used for anesthesia during radiotherapy. The rats were positioned with the right side down and covered with a lead shield designed to solely expose the left posterior mandible while protecting the remainder of the body.

The left hemimandibles underwent a 5-day fractionated external beam irradiation at the human equivalent radiation dosage of 70 Gy via a Philips RT250 orthovoltage unit (250 kV, 15 mA) (Kimtron Medical, Woodbury, CT). Our laboratory has previously established the protocol to deliver fractionated radiation that is equivalent to 70 Gy, the conventional dosing regimens for humans with HNC [8–11,35,36]. In addition this general radiation protocol has been performed for several years in the Department of Radiation Oncology under ULAM and UCUCA approved protocols [8–11,35,36].

Following radiation, the rats were provided soft chow and water ad libitum for 56 days. Rats received subcutaneous injection of Buprenorphine (0.15 m/kg) with 10 cm^3 lactated Ringer solution when showing signs of radiation-induced discomfort and/or pain [8–11,35,36].

Tissue harvesting

All animals survived and the left hemimandibles were harvested and frozen at −20 °C until imaging.

Raman spectroscopy

Raman spectra were obtained with a locally constructed micro-probe that has been previously described [12–18]. Briefly, a 785 nm diode laser (Invictus, Kaiser Optical Systems, Inc., Ann Arbor, MI) delivered approximately 250 mW line-focused radiation to the specimen through a microscope (E600, Nikon, Melville Station, NY) fitted with a 10×/0.5 NA objective (Nikon, S Fluor series). The backscattered Raman-shifted light was focused on the entrance slit of a spectrograph (HoloSpec, Kaiser Optical Systems, Inc.), operated at a 4 cm^{-1} resolution. The dispersed light was collected on a CCD (DU-401-BR-DD, Andor Technology, East Windsor, CT). Eight spectra were collected on the hemimandible surface over the region of interest previously described and established in our laboratory (Fig. 1) [8–11]. Both bone mineral and matrix-specific Raman bands were analyzed and band intensity ratios, such as carbonate/phosphate (1070 cm^{-1}/958 cm^{-1}) and mineral/matrix including the phosphate/phenylalanine (958 cm^{-1}/1002 cm^{-1}) and phosphate/(proline and hydroxyproline) (958 cm^{-1}/(854+873) cm^{-1}), collagen cross-link or matrix maturity (1660/1690 cm^{-1}) were calculated using GRAMS/AI software (Thermo Nicolet, Middleton, WI) (Table 1).

Overlapped bands were fitted to mixed Gaussian/Lorentzian functions in GRAMS. A fit to three bands was used for phosphate (PO_4^{3-}) ν_1. The phenylalanine/amide I region, 1580–1710 cm^{-1} was fitted to six bands. Only the intensities of the major components of amide I (approx. 1666 and 1686 cm^{-1}) were used to calculate the collagen cross-link (matrix maturity) ratio.

Statistics

One-way ANOVA with post-Tukey test was utilized for analysis of the aforementioned radiomorphometrics (PASW version 18; SSPS, Inc., Chicago, IL). Statistical significance was considered at a p value less than 0.05.

Results

Gross results

Following radiation, all animals recovered and survived. Although some animals in the AMF–XRT group experienced some weight loss (13%) during the radiation week, they significantly surpassed their original weight compared to the radiated and untreated rats. The

AMF pre-treated animals also displayed much less signs of radiation-induced stress, including alopecia and mucositis.

Upon harvest, significant loss of cortical density of the angular process of the mandibles was evidenced in the XRT group compared to the control and AMF pre-treated mandibles.

Raman spectra

We generated Raman spectra from the data collected from the surface of each murine hemimandible within our region of interest highlighted in Fig. 1. The results and attribution of the bands are detailed in Table 1 Part A. The Raman signatures of each group were clearly identified with the main band assignments for bone minerals and proteins as seen in Fig. 2. The most intense bands are attributed to the mineral part of the bone, such as phosphate ν(approx. 958 cm^{-1}), ν(588 cm^{-1}) and B-type carbonate (approx. 1070 cm^{-1}). The protein bands represent the organic part of the bone and consist mainly of the type I collagen. In the XRT rats, the intense phosphate P–O band at 958 cm^{-1} shifted about 0.25 cm^{-1} to a higher wavenumber compared to the same band in both the AMF–XRT group and the control group (Table 1, Part A and Fig. 2). Small band position shifts were observed between the three groups. XRT reduced the intensity of collagen bands relative to mineral. The collagen band intensity was only partially rescued by AMF. All derived spectroscopic parameters are shown in Table 1 Part B, while Fig. 3 summarizes the results in a graphical form to emphasize the partial rescue by AMF prophylaxis.

The full width at half maximum (FWHM) of the phosphate ν_1 band was decreased with XRT ($p \ll 0.05$, Fig. 3A), demonstrating an increase in mineral crystallinity. In the AMF–XRT group, FWHM of the phosphate ν_1 band showed no difference from that of the control ($p=0.248$; Fig. 3A), demonstrating an AMF rescue effect.

This finding is confirmed by the carbonate/phosphate ratio, which showed the same pattern. The ratio of carbonate/phosphate intensities for AMF–XRT showed no difference compared to that of the control ($p=0.147$); whereas the ratio for XRT was significantly different from those of the AMF and control groups ($p \ll 0.05$ and $p \ll 0.05$ respectively, Fig. 3B).

The mineral to matrix ratios were calculated as phosphate ν_1 intensity divided by the combined intensities of the proline and hydroxyproline bands ((854+873)cm^{-1}) and as phosphate ν_1 intensity divided by the intensity of the phenylalanine band (1002 cm^{-1}). The same results were obtained with both methods. Only the phosphate/phenylalanine data is shown in Fig. 3C. Significant differences were seen between all 3 groups for that parameter as well. In fact, the ratios for both XRT and AMF–XRT were increased compared to the control; however, the ratio for AMF–XRT was lower than the XRT ($p=0.014$) and closer to that of the control ($p=0.001$; Fig. 3C). In summary, XRT increased the mineral/matrix ratio and AMF only partially rescued this property.

The collagen cross-link or collagen maturity ratio (1660 cm^{-1}/1690 cm^{-1}) was increased from 2.8 to 4.1 by XRT. Importantly, AMF–XRT did not differ from XRT ($p=0.994$) but was significantly different from the control ($p=0.004$; Fig. 3D), showing that AMF prophylaxis left the pathological cross-linking largely unchanged.

To further illustrate the changes, the spectra from each group were averaged then the differences between XRT and control and AMF–XRT and control were calculated (Fig. 4). The major differentials between XRT and control occurred in both the mineral spectral region and in the protein spectral regions. With AMF prophylaxis, these spectral changes were not reproduced, particularly in the mineral part of the bone.

Discussion

Significant progress has been made in the field of radiation oncology in selectively targeting tumor cells while selectively sparing the normal adjacent tissue [37]. In the clinical arena of head and neck cancer (HNC), identifying such a “sensitizer” agent has been proven to be a key to improving the success and specificity of the treatment plan as well as enhancing the overall quality of care of the patient. In the craniofacial skeleton specifically, the cortical mandible is particularly at risk for the devastating effects of radiotherapy, where late pathologic fractures and osteoradionecrosis still represent a significant biomedical burden [38].

The authors have previously shown that radiation therapy induced damage to the murine mandible following a dose–response pattern [10,11]. The authors have also outlined a protocol that delivers a human equivalent dose of radiation (HEDR) that mirrors the total radiation dosage delivered to patients with HNC [9–11]. Furthermore, the author’s laboratory has investigated the effect of AMF pre-treatment in a murine mandibular model of distraction osteogenesis following the delivery of HEDR [35,36]. We demonstrated that AMF pre-treated mandibles showed evidence of strong bony union of the regenerate. Our gross findings were reproduced and quantified in both our histomorphometric data and mineralization radiomorphometrics, where the mean osteocyte count, the ratio of mature bone (bone volume/tissue volume), BVF, BMD, and TMD were significantly different in an AMF pre-treated group compared to an irradiated distracted group [35,36].

Subsequently, we focused our experiment to evaluate the effect of AMF on a non-distracted and irradiated mandible (with HEDR) using micro-computed tomography [8]. We demonstrated that AMF pre-treated specimens mirrored the control specimens and exhibited much less BVF, BMD and TMD compared to the radiated specimens. A closer look at the bone mineral density distribution histogram [39] showed that the irradiated specimens had a blunted remodeling and a shifted pattern towards hypermineralization. On the other hand, AMF seemed to enable the recruitment of more bone cells but only partially remediated the effects of radiation on the new bone formation [8]. In order to better understand how AMF functioned to protect the bone from the ravages of radiation we directed our query to specifically investigate the ability of this drug to preserve both the organic and inorganic components of bone in the same animal model. To investigate these compositional changes we employed Raman spectroscopy.

The microcharacterization of the cortical mandible bony constituents can provide a greater understanding of the pathophysiology of the events that occur when the bone undergoes radiation, and ultimately it may help circumvent the late effects of radiation on the bone, in particular pathologic fractures and osteoradionecrosis. Some molecular studies have reported radiation-induced changes within the mineral and organic components of the bone [40]. Evidence shows that irradiation alters the degree of cross-linking within the collagen [41,42]. This occurs as a result of side chain decarboxylation of the tissue, thus modifying the interaction or binding between the organic matrix and the hydroxyapatite mineral [42,43].

Utilizing Raman spectroscopy, we were able to better elucidate the changes induced by radiotherapy and the protective effect of AMF on the bone constituents.

We demonstrated major spectroscopic differences in the mineral composition of the bone where the irradiated tissue became hypermineralized, with an abnormally crystalline mineral. This was evidenced by both a shift in the position of the major phosphate band to a higher wavenumber and a decrease in the width of the band at 958 cm^{-1}. Indeed, mineral crystallinity is inversely proportional to the FWHM of phosphate. Therefore, the results

implied an increase in mineral crystallinity secondary to radiation. These effects were similar to the ones previously reported in human subjects by Lakshmi et al. [19]. It is also possible that the cell damage caused by radiation results in impaired and abnormal mineralization. It could be as simple as slowing the process, so that the resulting mineral has time to develop larger, less carbonated crystallites than normal–or there could be a more complicated mechanism that is yet to be investigated. AMF pre-treatment clearly restored those parameters to nearly the control levels. Similarly, there was no difference in the carbonate/phosphate ratio between AMF and the control ($p=0.147$); whereas the same ratio was significantly reduced for XRT. This finding highlights once again the protective effect of AMF against radiation-induced mineral damages in the murine mandible.

Quantification of the mineral/matrix ratio provides additional useful insight to the amount of mineralization and to evaluate compositional trends in the bone [12]. Phenylalanine, proline and hydroxyproline are the major amino acids contributing to the collagen or matrix content in our murine model. The changes observed in the mineral/matrix of the irradiated specimens suggest that either the mineral composition is increased and/or the matrix content is decreased. We have already demonstrated that the former is likely true where radiation affects the mineral composition of the bone. Kubisz et al. have shown that the content of selected amino acids in bone, including proline and hydroxyproline was significantly decreased with radiation exposure with a relative change that was higher for proline [20]. Our analysis of the ratios of phosphate divided by the combined proline and hydroxyproline mirrored the results obtained with the ratio of phosphate divided by phenylalanine. Such results allow us to conclude that radiation resulted in the diminution in the protein content. Interestingly, the results obtained with AMF–XRT showed some improvement compared to XRT; nonetheless, AMF–XRT differed from the control group. Those findings showed that AMF was not able to fully remediate the radiation-induced alterations in the mineralization content likely secondary to the interaction and role of both the major mineral phosphate and the matrix constituents.

The 1660/1690 cm^{-1} ratio in the amide I region corresponds to the ratio of non-reducible/reducible cross-links. The fact that no difference was observed between XRT and AMF–XRT ($p=0.954$) whereas both AMF–XRT and XRT significantly differed from the control ($p= 0.0004$ and $p=0.001$ respectively) indicates that the changes in cross-linking induced by radiation are not remediated by AMF. Although the correlations are complex, the amide band I changes with the secondary structure of the collagen backbone. It is difficult to quantify cross-links, but deviations from control values are good indicators that radiation changes the conformation of the collagen and AMF treatment does not result in complete rescue. Our findings reveal clues to both the strengths and limitations of AMF treatment and help to also tease out the mechanism of action by which the preservation of bone healing and regeneration occurs.

Overall, we can conclude that radiation affects both the mineral and organic matrix of the bone. AMF seems to specifically protect the mineral part of the bone. Amalgamating the results of this study with those of our previous reports, we may safely conclude that AMF mitigates the effect of radiation on bone at a cellular level and at the structural level of the mineral, thus substantially preserving bone quality, as well as maintaining the capacity for osseous regeneration and repair. Our data show that Raman spectroscopy can provide information that cannot readily be obtained by conventional histology or by X-ray techniques. Spectroscopy shows that changes in collagen cross-linking occur upon XRT and are not rescued by AMF. While the chemical composition of the cross-links is not available from the Raman data, their presence cannot be easily discerned by histology and is completely invisible to plain X-rays or CT. Similarly, abnormal mineral crystallinity is not reported by either histology or X-ray methods. These methodologies offer no clue to the

increased brittleness of irradiated tissue. That brittleness is consistent with the presence of extra cross-links that would inhibit sliding of collagen fibrils when the tissue is loaded.

A limitation of our study is that spectroscopic data were taken at only a single time point, 56 days post-irradiation. We have no spectroscopic information about immediate damage to the tissue or about the temporal progression of tissue repair, however our model was developed specifically for the adaptation and application to the clinical setting in order to improve outcomes where the final end points are of the most translational importance.

Conclusion

We report utilizing a novel approach of Raman spectroscopy to demonstrate the ability of AMF to prophylactically and specifically safeguard the inorganic component of the mandible bone from the pernicious effects of radiation induced injury. Furthermore we established the ability of Raman spectroscopy to reveal radiation-induced changes to both the organic and inorganic constituents of bone. Ongoing development of a noninvasive fiber optic Raman spectroscopy probe [12–18] holds the promise of moving this innovative technology from the bench to the bedside to both monitor the harmful effects of radiation on bone as well as the efficacy of therapeutic remediation using radioprotective drugs such as Amifostine.

Acknowledgments

We thank Mary Davis for her technical assistance in radiation.

Funding was provided by the National Institutes of Health grant RO1 CA 12587-01 to Steven R. Buchman and the National Institutes of Health grants R01 AR055222 and R01 AR056657 to Michael D. Morris.

References

[1]. Kalaycioglu M, Bukowski R. Clinical status of the new chemoprotective agent, Amifostine. Oncology. 1994; 8:15–23. [PubMed: 7522504]

[2]. Capizzi RL. Amifostine: the preclinical basis for broad-spectrum selective cytoprotection of normal tissues from cytotoxic therapies. Semin Oncol. 1996; 23(Suppl. 8):2–17. [PubMed: 8783661]

[3]. Foster-Nora JA, Siden R. Amifostine for protection from antineoplastic drug toxicity. Am J Health Syst Pharm. 1997; 54:787–800. [PubMed: 9099346]

[4]. Andreassen CN, Grau C, Lindegaard JC. Chemical radioprotection: a critical review of Amifostine as a cytoprotector in radiotherapy. Semin Radiat Oncol. 2003; 13(1):62–72. [PubMed: 12520465]

[5]. Mao J, Fatunase OA, Marks LB. Cytoprotection for radiation-associated normal tissue injury. Radiat Oncol Adv Cancer Treat Res. 2008; 139(4):302–22.

[6]. Brizel DM, Wasserman TH, Henke M, Strnad V, Rudat V, Monnier A, et al. Phase III randomized trial of Amifostine as a radioprotector in head and neck cancer. J Clin Oncol. 2000; 18:3339–45. [PubMed: 11013273]

[7]. Wasserman TH, Brizel DM, Henke M, Monnier A, Eschwege F, Sauer R, et al. Influence of intravenous Amifostine on xerostomia, tumor control, and survival after radiotherapy for head-and-neck cancer: 2-year follow-up of a prospective, randomized, phase III trial. Int J Radiat Oncol Biol Phys. 2005; 63(4):985–90. [PubMed: 16253773]

[8]. Tchanque-Fossuo CN, Donneys A, Deshpande SS, Farberg AS, Nelson NS, Boguslawski MJ, et al. Amifostine mitigates the untoward effects of radiation on the mineralization. Amifostine mitigates the untoward effects of radiation on the mineralization capacity of irradiated bone in the murine mandible. Plast Reconstr Surg. 2011; 127(5 S):83.

[9]. Monson LA, Farberg AS, Jing L, Buchman SR. Human equivalent radiation dose response in the rat mandible. Plast Reconstr Surg. 2009; 124(4 S):2.

[10]. Tchanque-Fossuo CN, Monson LA, Farberg AS, Donneys A, Zehtabzadeh AJ, Razdolsky ER, et al. Dose–response effect of human equivalent radiation in the murine mandible. Part I: a histomorphometric assessment. Plast Reconstr Surg. 2011; 128(1):1–8.

[11]. Tchanque-Fossuo CN, Monson LA, Farberg AS, Donneys A, Deshpande SS, Razdolsky ER, et al. Dose–response effect of human equivalent radiation in the murine mandible. Part II: a biomechanical assessment. Plast Reconstr Surg. 2011; 128(5):480–7.

[12]. Morris MD, Mandair GS. Raman assessment of bone quality. Clin Orthop Relat Res. 2010; 469:2160–9. [PubMed: 21116756]

[13]. Draper ERC, Morris MD, Camacho NP, Matousek P, Towrie M, Parker AW, et al. Novel assessment of bone using time-resolved transcutaneous Raman spectroscopy. J Bone Miner Res. 2005; 20:1968–72. [PubMed: 16234970]

[14]. Okagbare PI, Esmonde-White FWL, Goldstein SA, Morris MD. Development of noninvasive Raman spectroscopy for in-vivo evaluation of bone graft osseointegration in a rat model. Analyst. 2010; 135:3142–6. [PubMed: 20924520]

[15]. Schulmerich MV, Cole JH, Kreider JM, Edmonde-White FWL, Dooley KA, Goldstein SA, et al. Transcutaneous Raman spectroscopy of murine bone in vivo. Appl Spectrosc. 2009; 63:286–95. [PubMed: 19281644]

[16]. Srinivasan S, Schulmerich MV, Cole JH, Dooley KA, Kreider JM, Pogue BW, et al. Image-guided Raman spectroscopic recovery of canine cortical bone contrast in situ. Opt Express. 2008; 16(16):12190–200. [PubMed: 18679495]

[17]. Schulmerich MV, Srinivasan S, Cole JH, Kreider J, Dooley KA, Goldstein SA, et al. Non-invasive Raman tomographic imaging of canine cortical bone tissue. J Biomed Opt. 2008; 13(2): 020506. [PubMed: 18465948]

[18]. Macleod, NA.; Morris, MD.; Matousek, P. Characterisation of deep layers of tissue and powders: spatially offset Raman and transmission Raman spectroscopy. In: Matousek, Pavel; Morris, Michael D., editors. Emerging Raman applications and techniques in biomedical and pharmaceutical fields. Springer; Berlin: 2010. p. 47-69.

[19]. Lakshmi RJ, Alexander M, Kurien J, Mahato KK, Kartha VB. Osteoradionecrosis (ORN) of the mandible: a laser Raman spectroscopic study. Appl Spectrosc. 2003; 57:1100–16. [PubMed: 14611040]

[20]. Kubisz L, Polomska M. FT NIR Raman studies on irradiated bone. Spectrochim Acta Part A. 2007; 66(3):616–25. [66A].

[21]. Barth HD, Launey ME, MacDowell AA, Ager JW, Ritchie RO. On the effect of X-ray irradiation on the deformation and fracture behavior of human cortical bone. Bone. 2010; 46:1475–85. [PubMed: 20206724]

[22]. Posner AS. The crystal chemistry of bone mineral. Physiol Rev. 1969; 499(4):760–92. [PubMed: 4898602]

[23]. Posner AS. The mineral of bone. Clin Orthop. 1985; 200:87–99. [PubMed: 3905126]

[24]. Currey JD. Effects of differences in mineralization on the mechanical properties of bone. Philos Trans R Soc Lond B Biol Sci. 1984; 304(1121):509–18. [PubMed: 6142490]

[25]. Fratzl P, Gupta HS, Paschalis EP, Roschger P. Structure and mechanical quality of the collagen–mineral nano-composite in bone. J Mater Chem. 2004; 14:2115–23.

[26]. Currey JD. Role of collagen and other organics in the mechanical properties of bone. Osteoporos Int. 2003; 14(5 Suppl):S29–36. [PubMed: 14504703]

[27]. Katz EP, Wachtel E, Yamauichi M, Mechanic GL. The structure of mineralized collagen fibrils. Connect Tissue Res. 1989; 21:149–58. [PubMed: 2605938]

[28]. Olszta MJ, Cheng X, Jee SS, Kumar R, Kim YY, Kaufman MJ, et al. Bone structure and formation: a new perspective. Mater Sci Eng R. 2007; 58:77–116.

[29]. Jeon, JH.; Korlepara, VJ.; Blendell, J.; Akkus, O. Raman analysis of yield in cortical boneOptics in bone biology and diagnostics, 7166. SPIE; San Jose: 2009. p. 716606-716608.

[30]. Yerramshetty JS, Akkus O. The associations between mineral crystallinity and the mechanical properties of human cortical bone. Bone. 2008; 42(3):476–82. [PubMed: 18187375]

[31]. Akkus O, Adar F, Schaffler MB. Age-related changes in physicochemical properties of mineral crystals are related to impaired mechanical function of cortical bone. Bone. 2004; 34(3):443–53. [PubMed: 15003792]

[32]. Maher JR, Takahata M, Awad HA, Berger AJ. Raman spectroscopy detects deterioration in biomechanical properties of bone in a glucocorticoid-treated mouse model of rheumatoid arthritis. J Biomed Opt. 2011; 16(8):087012–6. [PubMed: 21895339]

[33]. Paschalis EP, Tatakis DN, Robins S, Fratzl P, Manjubala I, Zoehrer R, et al. Lathyrism-induced alterations in collagen cross-links influence the mechanical properties of bone material without affecting the mineral. Bone. 2011; 49(6):1232–41. [PubMed: 21920485]

[34]. Donnelly E, Boskey AL, Baker SP, Meulen MC. Effects of tissue age on bone tissue material composition and nanomechanical properties in the rat cortex. J Biomed Mater Res Part A. 2010; 92(3):1048–56.

[35]. Monson LA, Farberg AS, Jing XL, Tchanque-Fossuo CN, Donneys A, Buchman SR. Distraction osteogenesis in the rat mandible following radiation and treatment with Amifostine. Plast Reconstr Surg. 2010; 125(6):41.

[36]. Tchanque-Fossuo CN, Donneys A, Razdolsky ER, Monson LA, Farberg AS, Deshpande SS, et al. Quantitative histologic evidence of amifostine induced cytoprotection in an irradiated murine model of mandibular distraction osteogenesis. Plast Reconstr Surg. 2012; 130(6):1199–207. [PubMed: 22878481]

[37]. Poggi MM, Coleman N, Mitchell JB. Sensitizers and protectors of radiation and chemotherapy. Curr Probl Cancer. 2001; 25:329–412.

[38]. Chrcanovic BR, Reher P, Sousa AA, Harris M. Osteoradionecrosis of the jaws–a current overview–part 1: physiopathology and risk and predisposing factors. Oral Maxillofac Surg. 2010; 14:3–16. [PubMed: 20119841]

[39]. Nelson NS, Donneys A, Tchanque-Fossuo CN, Deshpande SS, Boguslawski MJ, Goldstein SA, et al. Normative reference parameters of bone mineral density distribution in the Sprague Dawley rat mandible. Plast Reconstr Surg. 2011; 127(5 S):61.

[40]. Currey JD, Foreman J, Laketic I, Mitchell J, Pegg DE, Reilly GC. Effects of ionizing radiation on the mechanical properties of human bone. J Orthop Res. 1997; 15:111–7. [PubMed: 9066534]

[41]. Bailey AJ, Rhodes DN, Cater CW. Irradiation-induced crosslinking of collagen. Radiat Res. 1964; 22(4):606–21. [PubMed: 14201872]

[42]. Bowes JH, Moss JA. The effect of gamma radiation on collagen. Radiat Res. 1962; 16:211–23. [PubMed: 13872073]

[43]. Burr DB. The contribution of the organic matrix to bone's material properties. Bone. 2002; 31(1): 8–11. [PubMed: 12110405]

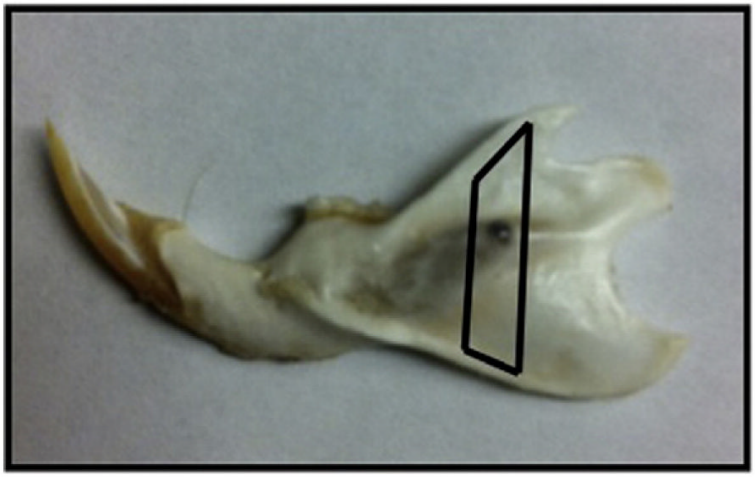

Fig. 1.
Murine hemimandible with the region of interest (ROI) highlighted in black. The laser was focused on the surface of the ROI and eight spectra were collected per hemimandible for analysis.

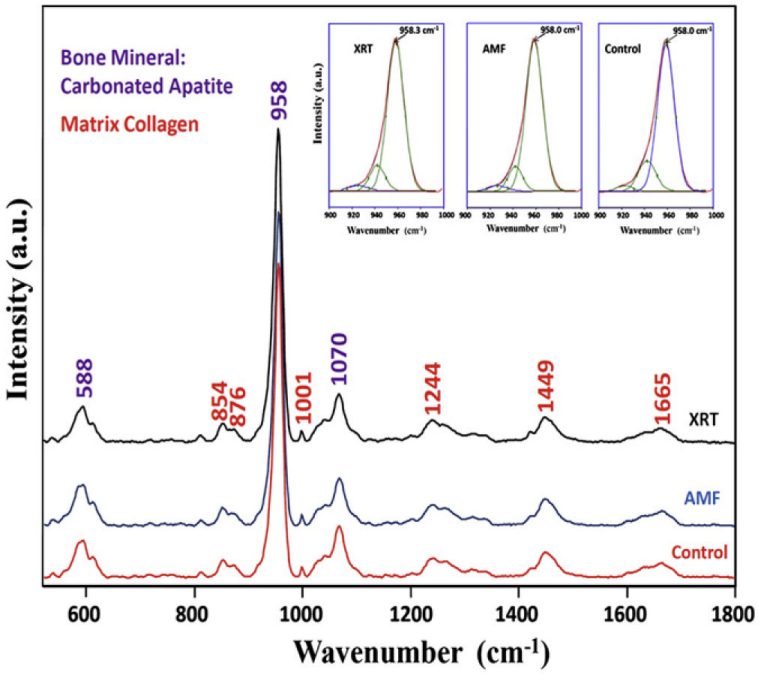

Fig. 2.

Murine mandible spectrum for a normal non-radiated bone (control), radiated (XRT) bone, and AMF pre-treated bone (AMF–XRT) with signature bands of bone mineral carbonated apatite and bone matrix collagen with minor contributions from other proteins, lipids, and glycosaminoglycans. Major bands of the mineral are marked in purple. Major bands of the matrix are marked in red.

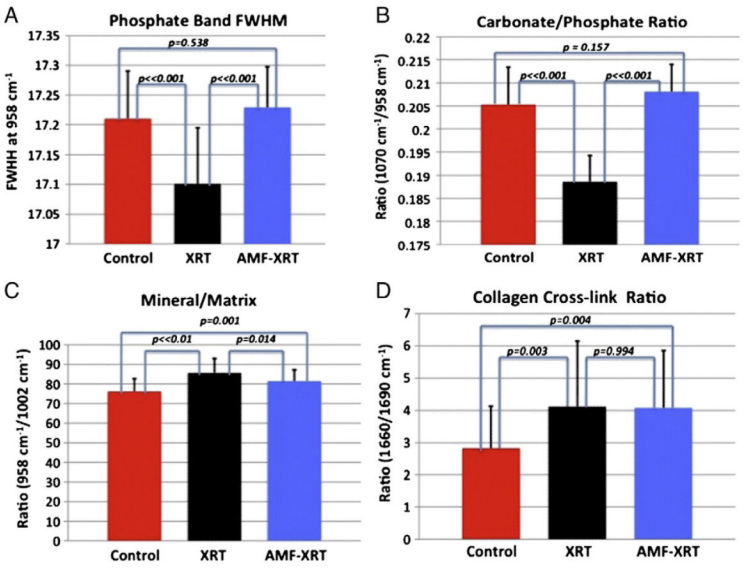

Fig. 3.

Comparisons of carbonate/phosphate ratio (A), phosphate/matrix ratio (B), collagen cross-link ratio (C) and full width at half maximum (FWHM) of the major phosphate band at 958 cm^{-1} (D) for the control, radiated (XRT), and Amifostine pre-treated (AMF–XRT) specimens.

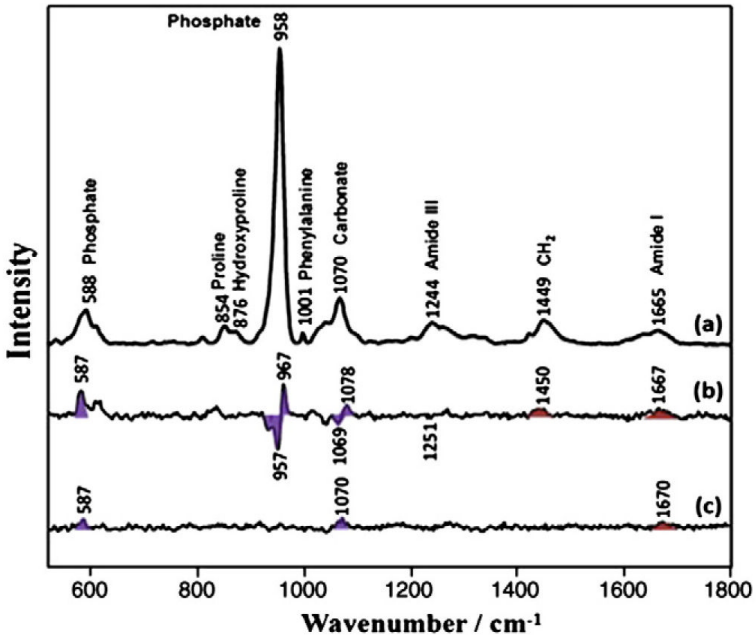

Fig. 4.

Raman spectra of control (a) and Raman difference spectra of [XRT] minus [control] (b) and [AMF] minus [control] (c). Major bands of the mineral are marked with violet shading. Major bands of the matrix are marked with red shading.

Table 1

Raman metrics

Part A. Raman band center wavenumber (BCW) and relative intensity (RI).

Groups	Phospate ν_1		Proline and Hydroxyproline		Phenylalanine		Carbonate	Subbands in amide I region	
	BCW (cm^{-1})	RI (a.u.)	BCW (cm^{-1})	RI (a.u.)	BCW (cm^{-1})	RI (a.u.)	BCW (cm^{-1})	BCW (cm^{-1})	RI (a.u.)
Control	957.99±0.01	17.43±0.22	853.09±0.07 874.28 ±0.09	1.84±0.11	1001.48±0.05	0.23±0.02	1070.74±0.15	1665.14±0.63 1685.61±0.40	1.27±0.38 0.50±0.18
XRT	958.26±0.06	17.55±0.17	852.64±0.39 873.63±0.79	1.66±0.08	1001.50±0.03	0.21±0.02	1070.60±0.21	1665.89±0.69 1686.73±0.56	1.09±0.31 0.30±0.11
AMF-XRT	958.05±0.05	17.19±0.22	852.92±0.10 874.07±0.24	1.71±0.07	1001.59±0.16	0.21±0.02	1070.74±0.15	1666.32±0.13 1686.45± 0.54	1.20±0.28 0.33±0.12

Part B. Derived spectroscopic parameters.

Groups	Mineral crystallinity FWHM PO_4^{3-} ν_1 ($958\ cm^{-1}$)	Carbonate/phosphate $1070\ cm^{-1}/958\ cm^{-1}$	Phosphate/phenylalanine $958\ cm^{-1}/1002\ cm^{-1}$	Phosphate/(proline and hydroxyproline) $958\ cm^{-1}/(854+873)\ cm^{-1}$	Collagen cross-link (matrix maturity) $1665\ cm^{-1}/1685\ cm^{-1}$
Control	17.21±0.08	0.21±0.01	76.16±6.49	9.51±0.51	2.83±1.30
XRT	17.10±0.09	0.19±0.01	85.66±7.36	10.62±0.51	4.12±2.03
AMF-XRT	17.23±0.09	0.21±0.01	81.44±5.80	10.07±0.39	4.08±1.77